Electronic Supplementary Material (ESI) for Journal of Materials Chemistry A.

Supporting information

A novel long-lasting antifouling membrane modified by bifunctional capsaicin-mimic moieties via in situ polymerization for efficient water purification

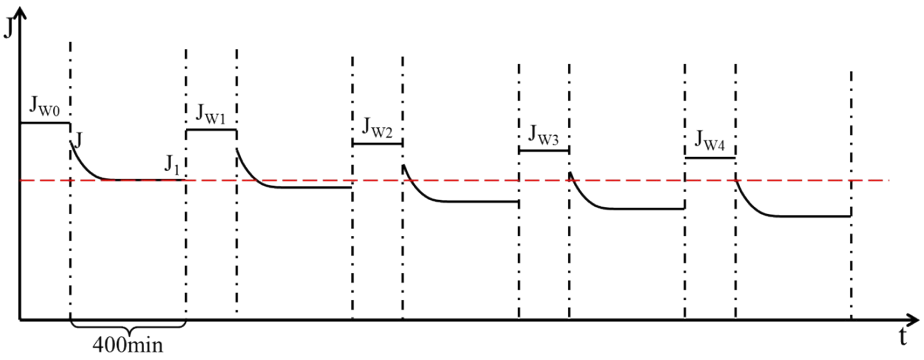

Fig. S1 Schematic diagram of filtration resistance analysis.

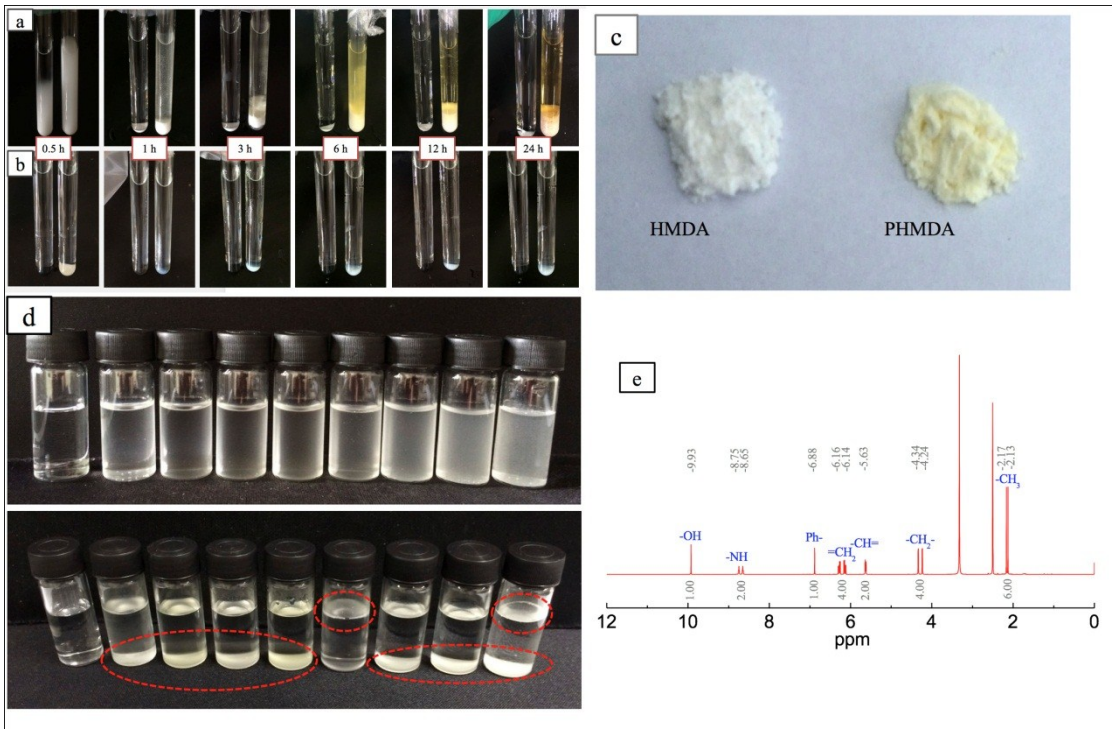

Fig. S2 HMDA self-polymerization in (a) ethanol and (b) DMAc. In each picture, the left tube contains no AIBN and the right tube contains AIBN. (c) Photos of the original HMDA and PHMDA. (d) Attempts to dissolve HMDA in various solvents for 5 days (above: suspension solution; and below: precipitation). The solvents are (from left to right): pure water (benchmark, no PHMDA), benzene, dimethylsulfoxide, dimethylacetamide, dimethyl formamide, CCl_3, retrahydrofuran, ethanol and water. (e) NMR results of the HMDA monomer.

As shown in Fig. S2a, the presence of AIBN in the right tube significantly promotes the self-polymerization in ethanol. Then we synthesized HMDA polymer in DMAc directly under the same condition (Fig. S2b). The preparation process of HMDA polymer is as follows: 3 g HMDA monomer and 0.15 g AIBN were added into 70.45 g DMAc. Simultaneously, a contrast experiment was designed without AIBN. These solutions were stirred for 24 h at 75 °C and then the obtained solutions were dropped into excess deionized water to precipitate the polymer. As shown in Fig. S2c, the polymer HMDA (PHMDA) was in yellowish color, and the attempt to dissolve the PHMDA in various solvents was unsuccessful after 5 days' continuous stirring, indicating the good organic solvent stability of the polymer (Fig. S2d).

In terms of the NMR results, the monomer HMDA was tested and the results are presented above. However, due to the difficulty in dissolving the PHMDA in various solvents, we failed to

obtain the NMR spectra for PHMDA polymer.

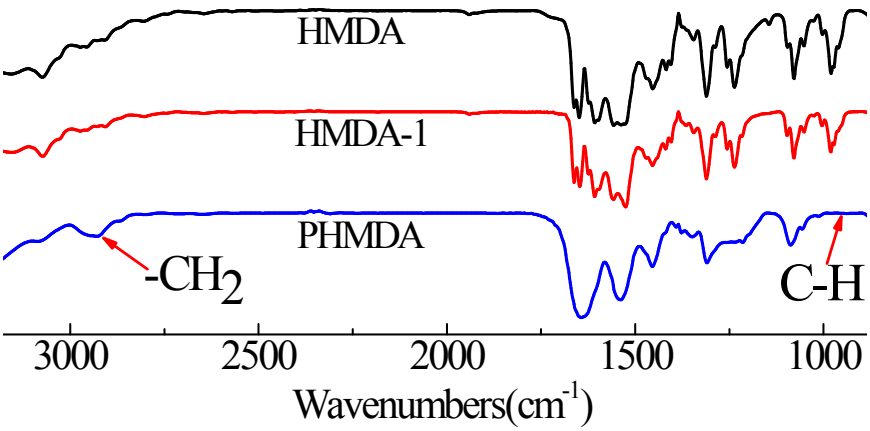

Fig. S3 FT-IR of HMDA and PHMDA polymer newly synthesized.

These chemical structures were analyzed by FT-IR. The FT-IR results are shown in Fig. S3. Addition of AIBN results in a clearly increasing at 2925 cm^{-1}, ascribed to the formation of CH_2 by the generation of PHMDA. Not surprisingly, FT-IR spectra of PHMDA present none absorption peaks at 995~985 cm^{-1}, assigned to C-H bending vibration bands of C=C. The bifunctional HMDA monomer has two C=C bond maybe polymerized partially, resulting in these TGA curve (Fig. 3b) essentially the same.

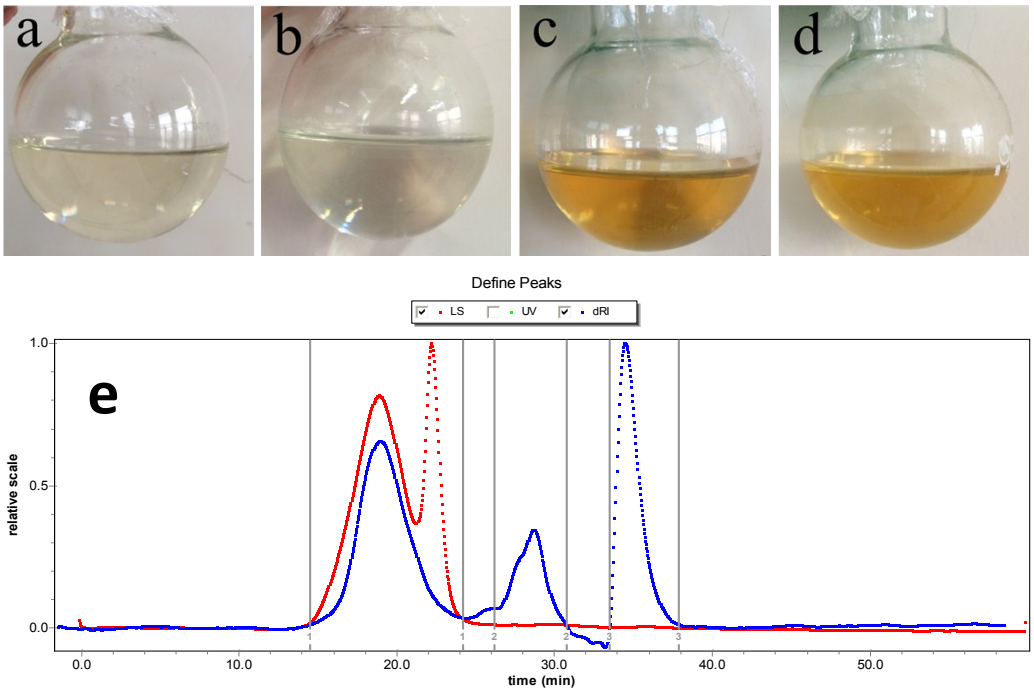

	Peak 1	Peak 2	Peak 3
Polydispersity			
Mw/Mn	1.259(3%)	1.357(83%)	1.325(73%)
Mz/Mn	2.208(5%)	2.797(140%)	3.829(142%)
Molar mass moments (g/mol)			
Mn	1.323e+5(2%)	6.173e+4(60%)	7.991e+3(48%)
Mp	1.146e+5(1%)	5.359e+4(53%)	6.436e+3(42%)
Mv	n/a	n/a	n/a
Mw	1.665e+5(2%)	8.378e+4(58%)	1.059e+4(55%)
Mz	2.921e+5(5%)	1.727e+5(127%)	3.060e+4(134%)

Fig. S4 Digital photos of membrane casting solutions (a) PSf, (b) A/PSf, (c) HMDA/PSf, (d) $HMDA_A$/PSf-3. (e) Size exclusion chromatography (SEC) results of the HMDAA/PSf-3 membrane casting solution (DMAc solvent).

In order to understand the molecular weight of the PHMDA within the membrane casting solution, we carried out the size exclusion chromatography (SEC) test with the membrane casting solution (DMAc solvent). The SEC results show two main peaks. The PSf polymer applied in this work has a molecular weight of around 50 kDa, indicating the peak 2 should be assigned to the PSf polymer. Subsequently, the peak 3 can be attributed to the PHMDA. The polymer has a Mn of ~7.99 kDa, with a polydispersity index (Mw/Mn) value of 1.325. This observation suggested the distribution of the polymer molecular weight is relatively narrow.

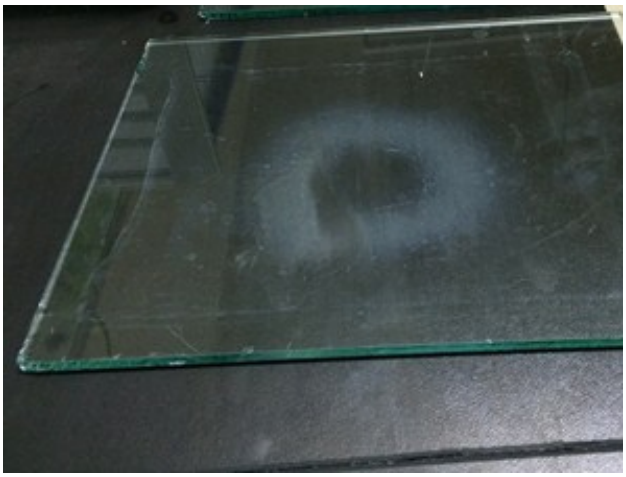

Fig. S5 Digital photos of glass pane used in the process of membrane preparation.

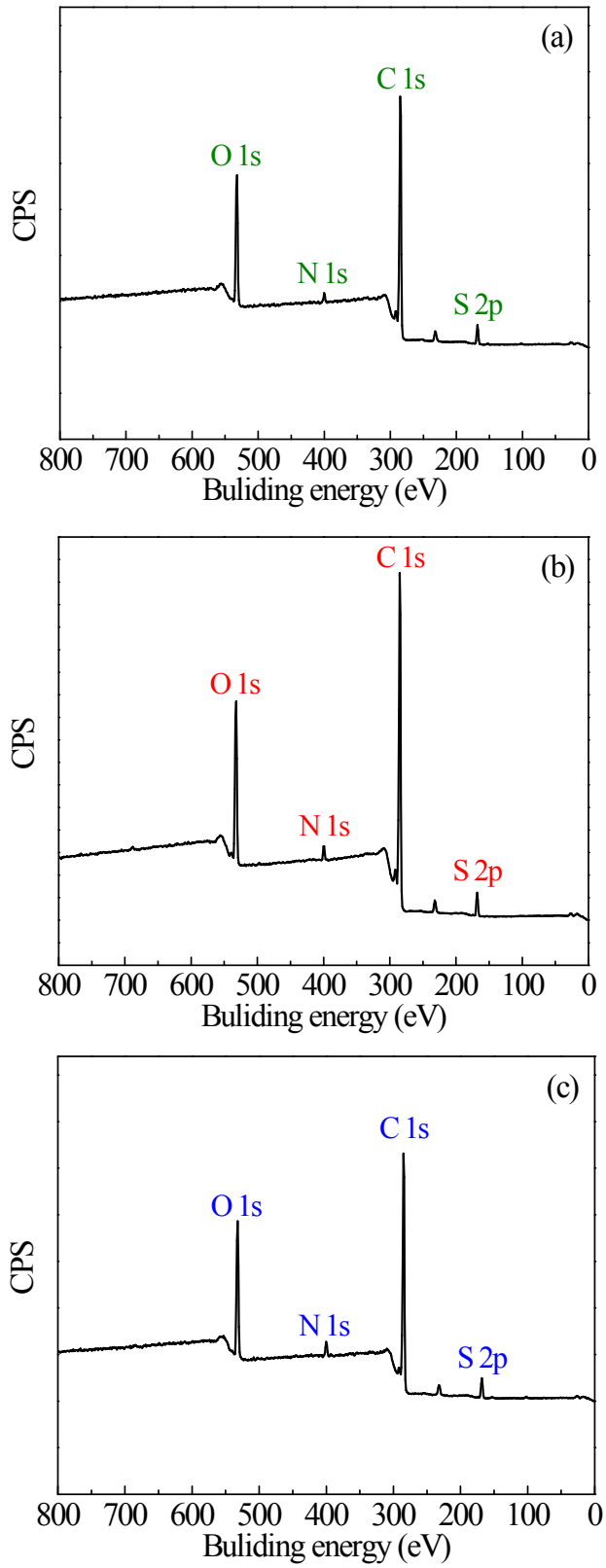

Fig. S6 XPS wide-scan spectrum for membrane surface (a) fresh PSf membrane, (b) fresh $HMDA_A$/PSf-3 membrane, (c) $HMDA_A$/PSf-3 membrane exposed to air for 2 months.

Calculations of the theoretical value:

As shown in PSf molecules ($C_{27}H_{22}O_4S$), the number of sp^3C in a unit is 3 and the total number of C1s in a unit is 27. Then theoretical sp^3C contents on the PSf membrane surface was caculated (11.11%). The number of sp^3C in a HMDA molecule is 6 when HMDA polymerized partially, and that of HMDA polymerized totally is 8. Then theoretical sp^3C contents on the $HMDA_A$/PSf-3 membrane surface was caculated (14.58%~16.23%). Threrefore, compared with the virgin PSf membrane, the theoretical sp^3C contents on the $HMDA_A$/PSf-3 membrane surface increased by 31.23% ~ 46.08%.

Calculations of the actual value:

Actual sp^3C contents caculated by XPS on the membrane surface of PSf and $HMDA_A$/PSf-3 were 14.92% and 16.95%, respectively. Threrefore, compared with the virgin PSf membrane, the actual sp^3C contents on the $HMDA_A$/PSf-3 membrane surface increased by 13.61%.

Actual sp^3C contents on the PSf membrane surface was 14.92% which is slightly higher than that of theoretical value (~11.11%). According to the actual increase rate of 13.61% and excluding deviation, we got the sp^3C contents on the $HMDA_A$/PSf-3 membrane surface was 12.62%. Threrefore, the content of HMDA on $HMDA_A$/PSf-3 was 6.25 wt% when HMDA polymerized partially. According to the same algorithm, the content of HMDA on $HMDA_A$/PSf-3 when HMDA polymerized totally was 4.25 wt%.

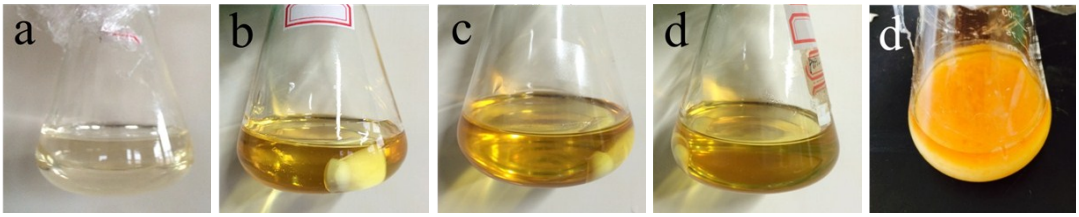

Fig. S7 Digital photos of membrane casting solutions. (a) 0 wt%, (b) 1 wt%, (c)2 wt%, (d)3 wt%, (e) 5 wt%.

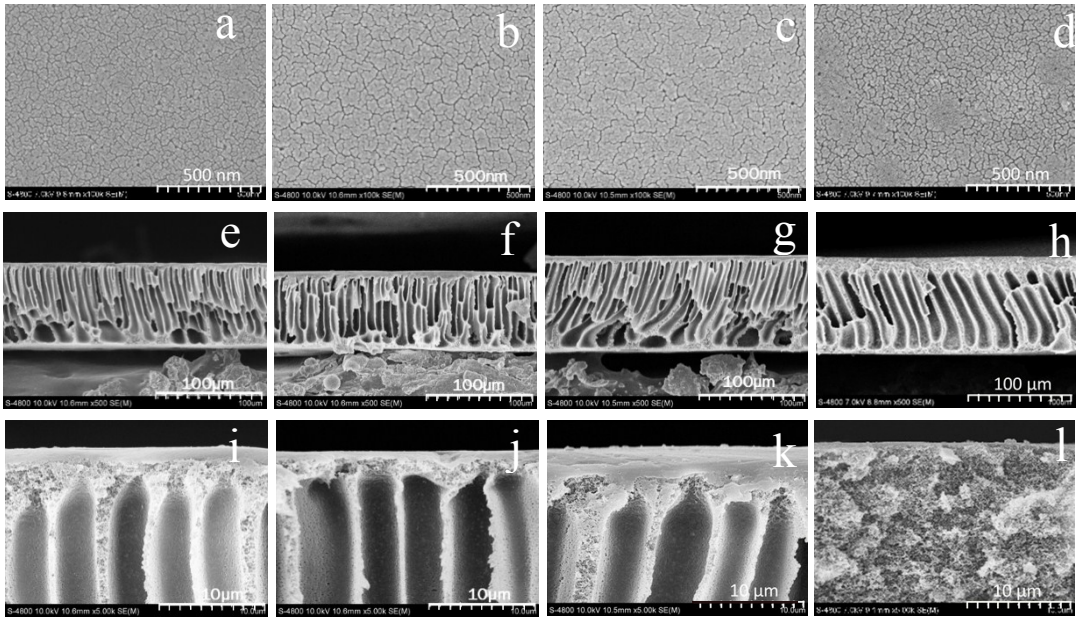

Fig. S8 SEM images for the membrane. (a,e,i) PSf, (b,f,j) A/PSf, (c,g,k) HMDA/PSf, (d,h,l) $HMDA_A$/PSf-3.

Fig. S8 represents the SEM images of PSf, A/PSf, HMDA/PSf and $HMDA_A$/PSf-3 membranes. As shown in Fig. S8 (a,e,i), the incorporation of HMDA or AIBN exerted little influence on the surface morphology of membranes. The wet phase inversion process typically generated asymmetric membranes. In this research, compared with control PSf membrane, all the membranes shown the similar cross-sectional morphologies with a dense thin top layer, a puff sponge-like structure layer and a porous finger-like sub-layer. With the incorporation of HMDA and AIBN the thickness of puff sponge-like structure layer have increased, indicating the anti-fouling membrane was prepared successfully.

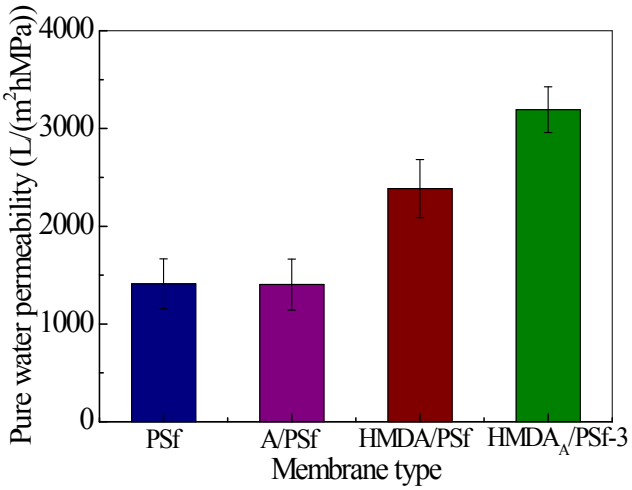

Fig. S9 Pure water permeability of various of membranes.

As shown in Fig. S9, $HMDA_A$/PSf-3 membrane with a water permeability of 3192 L/m^2hMPa which was two times higher than that of PSf membrane (1411 L/m^2hMPa). One possible reason for the difference in the permeability may be due to the changes of SEM cross-section, which caused by the incorporation of HMDA and AIBN.

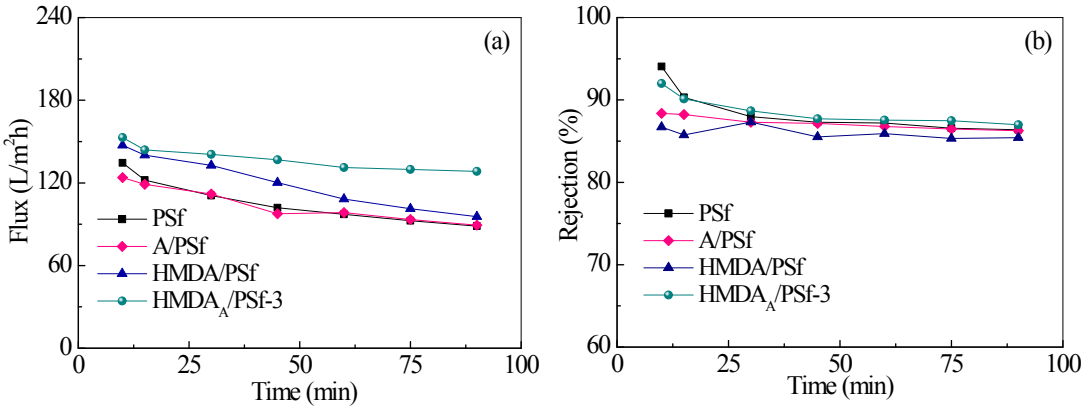

Fig. S10 Permeation flux (a) and Rejection (b) of membranes for ultrafiltration of HA solution.

Fig. S10 shows the permeation flux of and rejection to 5 mg/L HA solution at an operation pressure of 0.1 MPa. Similar to the results of pure water permeability observed above, $HMDA_A$/PSf-3 yielded a higher permeation flux than the pristine PSf membrane as far as the filtration of HA solution is concerned. A 44.8% improvement in the steady-state permeation flux was achieved by adding HMDA and AIBN to the PSf membrane, which may be attributed largely to the cellular structure of this membrane.

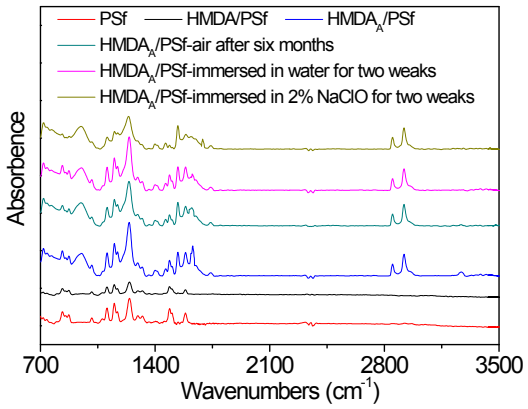

Fig. S11 FT-IR spectra of the membrane with different treatment.